UCRL-CONF-232604

LAWRENCE LIVERMORE NATIONAL LABORATORY

Long-Term Corrosion Testing of Thermal Spray Coatings of Amorphous Metals: Fe49.7Cr17.7Mn1.9Mo7.4W1.6B15.2C3.8Si2... and Fe48Mo14Cr15Y2C15B6

J.C. Farmer, D. Day, T. Lian, C-K. Saw, P. Hailey, J. Payer, L. Aprigliano, B. Beardsley, D. Branagan

July 9, 2007

Disclaimer

Long-Term Corrosion Testing of
Thermal Spray Coatings of Amorphous Metals:
$Fe_{49.7}Cr_{17.7}Mn_{1.9}Mo_{7.4}W_{1.6}B_{15.2}C_{3.8}Si_{2.4}$ and $Fe_{48}Mo_{14}Cr_{15}Y_2C_{15}B_6$

J. Farmer, S. Day, T. Lian, C-K. Saw and P. Hailey
Lawrence Livermore National Laboratory, Livermore, California USA

J. Payer
Case Western Reserve University, Cleveland, Ohio USA

L. Aprigliano
Strategic Analysis, Arlington, Virginia USA

B. Beardsley
Caterpillar, Peoria, Illinois USA

D. Branagan
The NanoSteel Company, Idaho Falls, Idaho USA

Abstract

Amorphous alloys identified as SAM2X5 ($Fe_{49.7}Cr_{17.7}Mn_{1.9}Mo_{7.4}W_{1.6}B_{15.2}C_{3.8}Si_{2.4}$) and SAM1651 ($Fe_{48}Mo_{14}Cr_{15}Y_2C_{15}B_6$) have been produced as melt-spun ribbons, drop-cast ingots and thermal-spray coatings. Chromium (Cr), molybdenum (Mo) and tungsten (W) additions provided corrosion resistance, while boron (B) enabled glass formation. Earlier electrochemical studies of melt-spun ribbons and ingots of these amorphous alloys demonstrated outstanding passive film stability. More recently thermal-spray coatings of these amorphous alloys have been made and subjected to long-term salt-fog and immersion tests. Good corrosion resistance has been observed during salt-fog testing. Corrosion rates were measured in situ with linear polarization, while simultaneously monitoring the open-circuit corrosion potentials. Reasonably good performance was observed. The sensitivity of these measurements to electrolyte composition and temperature was determined. The high boron content of SAM2X5 also made it an effective neutron absorber, and suitable for criticality control applications.
.

Introduction

The outstanding corrosion that may be possible with amorphous metals was recognized several years ago [1-3]. Compositions of several iron-based amorphous metals were published, including several with very good corrosion resistance. Examples included thermally sprayed coatings of Fe-10Cr-10-Mo-(C,B), bulk Fe-Cr-Mo-C-B, and Fe-Cr-Mo-C-B-P [4-6]. The corrosion resistance of an iron-based amorphous alloy with yttrium (Y), $Fe_{48}Mo_{14}Cr_{15}Y_2C_{15}B_6$ was also been established [7-9]. Yttrium was added to this alloy to lower the critical cooling rate.

Several nickel-based amorphous metals were developed that exhibit exceptional corrosion performance in acids, but are not considered in this study, which focuses on iron-based amorphous metals. Very good thermal spray coatings of nickel-based crystalline coatings were deposited with thermal spray, but appear to have less corrosion resistance than nickel-based amorphous metals [10].

A family of iron-based amorphous metals with very good corrosion resistance was developed that can be applied as a protective thermal spray coating. One of the most promising formulations within this family was found to be $Fe_{49.7}Cr_{17.7}Mn_{1.9}Mo_{7.4}W_{1.6}B_{15.2}C_{3.8}Si_{2.4}$ (SAM2X5), which included chromium (Cr), molybdenum (Mo), and tungsten (W) for enhanced corrosion resistance, and boron (B) to enable glass formation and neutron absorption. The parent alloy for this series of amorphous alloys, which is known as SAM40 and represented by the formula $Fe_{52.3}Cr_{19}Mn_2Mo_{2.5}W_{1.7}B_{16}C_4Si_{2.5}$, has less molybdenum than SAM2X5 and was originally developed by Branagan [11-12]. SAM2X5 may have beneficial for applications such as the safe long-term storage of spent nuclear fuel [13-16].

Experimental

Thermal Spray Coatings

The coatings discussed here were made with the high-velocity oxy-fuel (HVOF) process, which involves a combustion flame, and is characterized by gas and particle velocities that are three to four times the speed of sound (mach 3 to 4). This process is ideal for depositing metal and cermet coatings, which have typical bond strengths of 5,000 to 10,000 pounds per square inch (5-10 ksi), porosities of less than one percent (< 1%) and extreme hardness. The cooling rate that can be achieved in a typical thermal spray process such as HVOF are on the order of ten thousand Kelvin per second (10^4 K/s), and are high enough to enable many alloy compositions to be deposited above their respective critical cooling rate, thereby maintaining the vitreous state. However, the range of amorphous metal compositions that can be processed with HVOF is more restricted than those that can be produced with melt spinning, due to the differences in achievable cooling rates. Both kerosene and hydrogen have been investigated as fuels in the HVOF process used to deposit SAM2X5.

X-Ray Diffraction

The basic theory for X-ray diffraction (XRD) of amorphous materials is well developed and has been published in the literature [17-18]. In an amorphous material, there are broad diffraction peaks. During this study, XRD was done with CuK_α X-rays, a graphite analyzing crystal, and a Philips vertical goniometer, using the Bragg-Bretano method. The X-ray optics were self-focusing, and the distance between the X-ray focal point to the sample position was equal to the distance between the sample position and the receiving slit for the reflection mode. Thus, the intensity and resolution were optimized. Parallel vertical slits were added to improve the scattering signal. Step scanning was performed from 20 to 90° (2θ) with a step size of 0.02° at 4 to 10 seconds per point, depending on the amount of sample. The samples were loaded into low-quartz holders because the expected intensity was very low, thus requiring that the background scattering be minimized.

Salt Fog Testing

Salt fog tests were conducted according to the standard General Motors (GM) salt fog test, identified as GM9540P. The protocol for this test is summarized in Table 1. The salt solution mists consisted of 1.25% solution containing 0.9% sodium chloride, 0.1% calcium chloride, and 0.25% sodium bicarbonate. The four reference samples were Type 316L stainless steel, nickel-based Alloy C-22, Ti Grade 7, and the 50:50 nickel-chromium binary.

Table 1. A description of the standard GM9540P Salt Fog Test is summarized here. Note that the salt solution mists consisted of 1.25% solution containing 0.9% sodium chloride, 0.1% calcium chloride, and 0.25% sodium bicarbonate.

24-Hour Test Cycle for GM9540P Accelerated Corrosion Test		
Shift	Elapsed Time (hrs)	Event
Ambient Soak	0	Salt solution mist for 30 seconds, followed by ambient exposure at 13-28°C (55-82°F)
	1.5	Salt solution mist for 30 seconds, followed by ambient exposure at 13-28°C (55-82°F)
	3	Salt solution mist for 30 seconds, followed by ambient exposure at 13-28°C (55-82°F)
	4.5	Salt solution mist for 30 seconds, followed by ambient exposure at 13-28°C (55-82°F)
Wet Soak	8 to 16	High humidity exposure for 8 hours at 49 ± 0.5°C (120 ± 1°F) and 100% RH, including a 55-minute ramp to wet conditions
Dry Soak	16 to 24	Elevated dry exposure for 8 hours at 60 ± 0.5°C (140 ± 1°F) and less than 30% RH, including a 175-minute ramp to dry conditions

Corrosion Rate Determination During Immersion Testing

The linear polarization method was used as a method for determining the corrosion rates of the various amorphous metal coatings. The procedure used for linear polarization testing consisted of the following steps: (1) holding the sample for ten seconds at the open-circuit potential (OCP); (2) beginning at a potential 20 mV below the OCP, increasing the potential linearly at a constant rate of 0.1667 mV per second to a potential 20 mV above the OCP; (3) recording the current being passed from the counter electrode to the working electrode as a function of potential relative to a standard Ag/AgCl reference electrode; and (4) determining the parameters in the cathodic Tafel line by performing linear regression on the voltage-current data, from 10 mV below the OCP, to 10 mV above the OCP. The slope of this line was the polarization resistance, R_p (ohms), as defined in the published literature [19].

$$R_P = \left(\frac{\partial E}{\partial I} \right)_{E_{corr}} \tag{1}$$

A parameter (B) was defined in terms of the anodic and cathodic slopes of the Tafel lines, β_a and β_c, respectively:

$$B = \frac{\beta_a \beta_c}{2.303(\beta_a + \beta_c)} \qquad (2)$$

Values of B were published for a variety of iron-based alloys, and varied slightly from one alloy-environment combination to another [19]. Values for carbon steel, as well as Type 304, 304L and 430 stainless steels, in a variety of electrolytes which include seawater, sodium chloride, and sulfuric acid, ranged from 19 to 25 mV. A value for nickel-based Alloy 600 in lithiated water at 288°C was given as approximately 24 mV. While no values have yet been developed for the Fe-based amorphous metals that are the subject of this investigation, it is believed that a conservative representative value of approximately 25 mV is appropriate for the conversion of polarization resistance to corrosion current. Given the value for Alloy 600, a value of 25 mV was also believed to be acceptable for converting the polarization resistance for nickel-based Alloy C-22 to corrosion current. The corrosion current density, i_{corr} (A cm^{-2}), was defined in terms of the Tafel parameter (B), the polarization resistance (Rp), and the actual electrode area (A):

$$i_{corr} = \frac{B}{R_p \times A} \qquad (3)$$

The corrosion (or penetration) rates of the amorphous alloy and reference materials were calculated from the corrosion current densities with the following formula:

$$\frac{dp}{dt} = \frac{i_{corr}}{\rho_{alloy} n_{alloy} F} \qquad (4)$$

where p is the penetration depth, t is time, i_{corr} is the corrosion current density, ρ_{alloy} is the density of the alloy (g cm^{-3}), n_{alloy} is the number of gram equivalents per gram of alloy, and F is Faraday's constant. The value of n_{alloy} was calculated with the following formula:

$$n_{alloy} = \sum_j \left(\frac{f_j n_j}{a_j} \right) \qquad (5)$$

where f_j is the mass fraction of the jth alloying element in the material, n_j is the number of electrons involved in the anodic dissolution process, and a_j is the atomic weight of the jth alloying element. Congruent dissolution was assumed, which meant that the dissolution rate of a given alloy element was proportional to its concentration in the bulk alloy. These equations were used to calculate factors for the conversion of corrosion current density to the penetration rate (corrosion rate).

Standard Test Solutions Used for Immersion Testing

In addition to natural seawater and 3.5-molal sodium chloride solutions, several standardized test solutions have been developed based upon the well J-13 water composition determined by Harrar et al. [20]. Relevant test environments are assumed to include simulated dilute water (SDW), simulated concentrated water (SCW), and simulated acidic water (SAW) at 30, 60, and 90°C. The compositions of all of the environments are given in Table 2. The compositions of these test media are based upon the work of Gdowski et al. [21-23]. In general, anions such as chloride promote localized corrosion, whereas other anions such as nitrate tend to act as corrosion inhibitors. Thus, there is a very complex synergism of corrosion effects in the test media.

Table 2. Composition of Standard Test Media Based Upon Well J-13 Water

Ion	SDW	SCW	SAW
	(mg/L^{-1})	(mg/L^{-1})	(mg/L^{-1})
K^{+1}	34	3,400	3,400
Na^{+1}	409	40,900	40,900
Mg^{+2}	1	1	1,000
Ca^{+2}	1	1	1,000
F^{-1}	14	1,400	0
Cl^{-1}	67	6,700	6,700
NO_3^{-1}	64	6,400	6,400
SO_4^{-2}	167	16,700	16,700
HCO_3^{-1}	947	70,000	0
Si (60°C)	27	27	27
Si (90°C)	49	49	49
pH	8.1	8.1	2.7

Results

Crystalline and Amorphous Powders and Coatings

X-ray diffraction (XRD) data for SAM2X5 gas-atomized powders are shown in Figure 1. These powders are identified as (a) Lot # 05-079 and and (b) Lot # 06-015. The data for Lot # 05-079 show the formation of deleterious crystalline phases, including Cr_2B, WC, $M_{23}C_6$ and bcc ferrite, whereas the data for Lot # 06-015 show broad halos at $2\theta \sim 44°$ and $78°$, which are indicative of amorphous powder (absence of residual crystalline structure). These two lots of powder were used to prepare the thermal-spray coatings tested during this study.

XRD data for the corresponding SAM2X5 thermal-spray coatings are shown in Figure 2. The left frame (a) shows XRD for the coating produced with Lot # 05-079 powder and deposited on Type 316L stainless steel substrate. The broad halo at $2\theta \sim 44°$ is attributed to the presence of an amorphous matrix, while the sharp pronounced peaks are attributed to the presence of Cr_2B, WC, $M_{23}C_6$ and bcc ferrite, which are believed to have a detrimental effect on corrosion resistance. These deleterious precipitates deplete the amorphous matrix of those alloying

elements, such as Cr, Mo and W responsible for enhanced passivity. The distinctive satellite peak at 2θ ~ 36° may be due to the formation of tungsten carbide during the thermal spray process. The structure seen near 2θ ~ 60° may be due to bcc ferrite, and has been correlated with increased susceptibility of such amorphous metal coatings to corrosion. Other structure is due to $M_{23}C_6$ and Cr_2B. Coatings with less residual crystalline phase have been successfully produced, and will be discussed subsequently. The right frame (b) shows XRD data for the coating produced with Lot # 06-015 powder, and deposited on a Type 316L stainless steel substrate, identified as Sample # E316L511. Here too the broad halo observed at 2θ ~ 44° is attributed to the presence of an amorphous matrix. This coating appears to have less residual crystalline structure than the one produced with Lot # 05-079 powder.
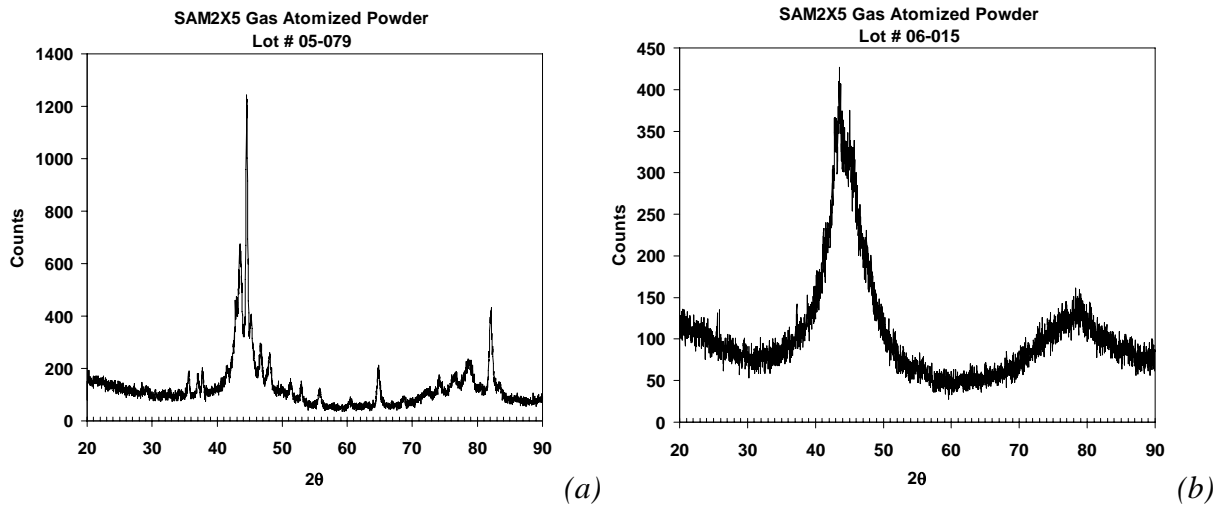

Figure 1. (a) XRD data for SAM2X5 ($Fe_{49.7}Cr_{17.7}Mn_{1.9}Mo_{7.4}W_{1.6}B_{15.2}C_{3.8}Si_{2.4}$) powder identified as Lot # 05-079. (b) XRD data for SAM2X5 powder identified as Lot # 06-015.
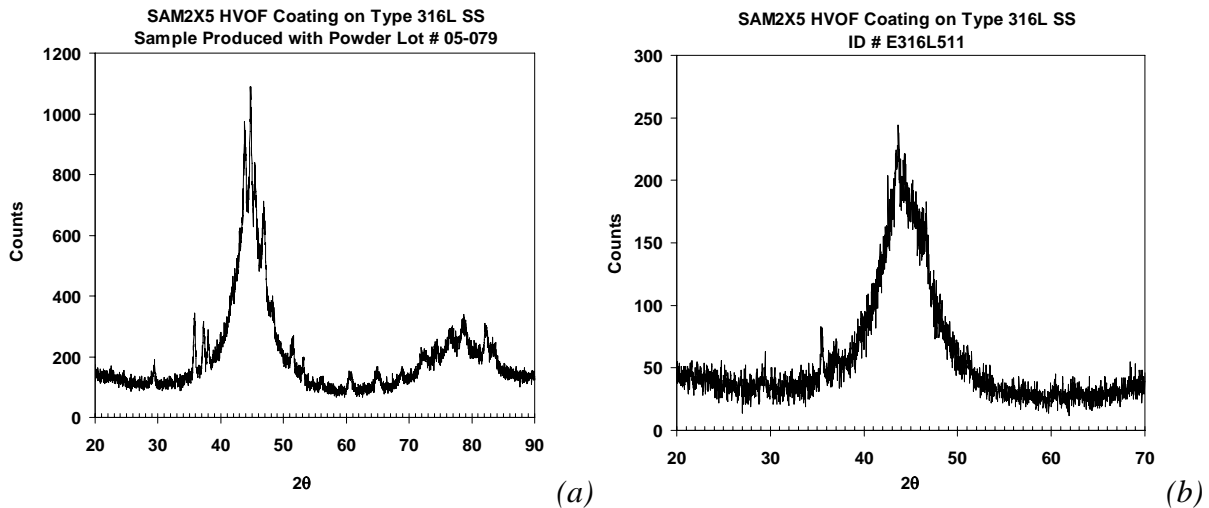

Figure 2. (a) XRD data for SAM2X5 coating (powder lot # 05-079) on Type 316L stainless steel substrate. (b) XRD data for SAM2X5 coating (powder lot # 06-015) on Type 316L stainless steel substrate (sample # E316L511).

Salt Fog Performance

Photographs of samples after eight full cycles in the GM salt-fog test described in Table 1 are shown in Figure 3. These samples are: (a) 1018 carbon steel reference specimens [Samples # A14]; (b) HVOF coating of SAM2X5 on Type 316L stainless steel substrate [Sample # 316L-W9], and HVOF coating of SAM2X5 on nickel-based Alloy C-22 substrate [Sample # C22-W21] after 8 full cycles in GM salt fog test. Clearly, the thermal-spay coatings of SAM2X5 have good resistance to corrosive attack in such environments.
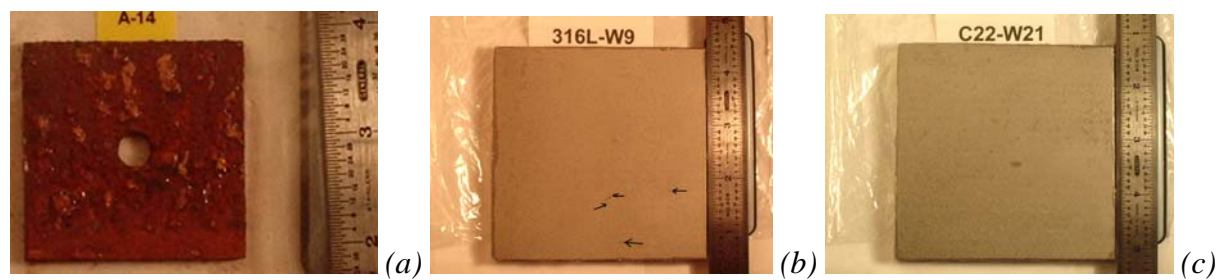

(a)   *(b)*   *(c)*

Figure 3. Photographs of three samples after eight full cycles in the GM salt-fog test: (a) 1018 carbon steel reference sample; (b) SAM2X5 Lot # 06-015 on 316L; and SAM2X5 Lot # 06-015 on Alloy C-22.

Corrosion Rates with Linear Polarization

Corrosion rates and open-circuit corrosion potentials of HVOF SAM2X5 and SAM1651 coatings were determined in situ during long-term immersion testing in several relevant environments and are reported here. SAM2X5 coatings were produced with both amorphous and partially devitrified powder. Powder produced 2006 (Lot #06-015) was amorphous whereas powder produced in 2005 (Lot #05-079) was partially devitrified due to problems encountered with the gas atomization process. All SAM1651 powder was amorphous. Figure 4 shows OCP values for the amorphous and partially devitrified SAM2X5 coatings. Coatings prepared with amorphous powder (Lot # 06-015) had relatively low OCP values in seawater at 90°C (−275 to −300 mV), whereas coatings produced with partially devitrified powder (Lot # 05-079) had slightly higher values (−230 mV). Coatings prepared with amorphous powder (Lot #06-015) also had relatively low OCP values in 3.5-molal NaCl solution at 90°C (−290 mV), whereas coatings produced with partially devitrified powder (Lot # 05-079 powder) had higher values (−260 mV). The trend in OCP appears to have reversed in 3.5-molal NaCl solutions at 30°C.

Figure 5 shows values of the corrosion rate determined with linear polarization during long-term open circuit corrosion testing of SAM2X5 coating samples prepared with lots of powder produced in 2004, 2005 and 2006. Coatings produced with completely amorphous SAM2X5 powder (Lot # 06-015) had relatively low corrosion rates in seawater at 90°C (~1.5 μm/yr). In contrast, coatings produced with partially devitrified SAM2X5 powder (Lot # 05-079) had relatively high corrosion rates (~4.7 μm/yr). Similarly, SAM2X5 coating samples produced with Lot # 06-015 powder exhibited relatively low LPCR values in 3.5-molal NaCl solution at 90°C (~21.1 μm/yr), in comparison to those samples with Lot # 05-079 powder (~107.2 μm/yr). Measurements of linear-polarization corrosion rate in 3.5-molal NaCl solution at 30°C were very

similar for SAM2X5 coating samples produced with Lots # 06-015 and # 05-079 (~2.7 and 3.6 µm/yr, respectively). Since these as-sprayed samples were very rough, an estimated roughness factor of 3.36 was used to convert apparent surface area to actual surface area.

Figures 6 and 7 show OCP values and corrosion rates for amorphous SAM2X5 (Lot #06-015) and SAM1651 coatings in seawater, 3.5-molal NaCl solutions, and synthetic bicarbonate brines (SDW, SCW and SAW). Based upon the corrosion rates of SAM2X5 coatings, solutions are ranked from least- to most-aggressive: SDW at 90°C; 3.5-molal NaCl with 0.525-molal KNO3 solution at 90°C; seawater at 90°C; 3.5-molal NaCl solution at 30°C; SCW at 90°C; SAW at 90°C; and 3.5-molal NaCl solution at 90°C. The ranking for SAM1651 coatings are slightly different. SAM1651 may perform better than SAM2X5 in hot 3.5-molal NaCl solution.
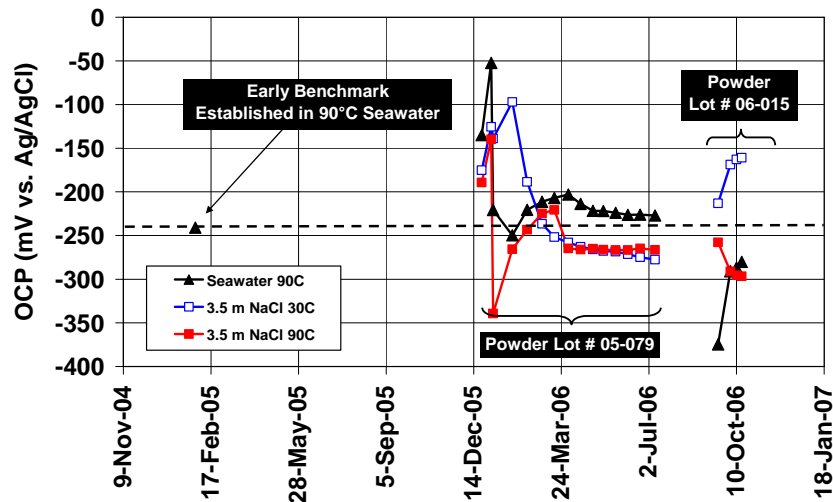

Figure 4. OCP values during long-term open circuit corrosion testing of as-sprayed SAM2X5 coatings prepared with Lot #05-079 and Lot #06-015 powders.
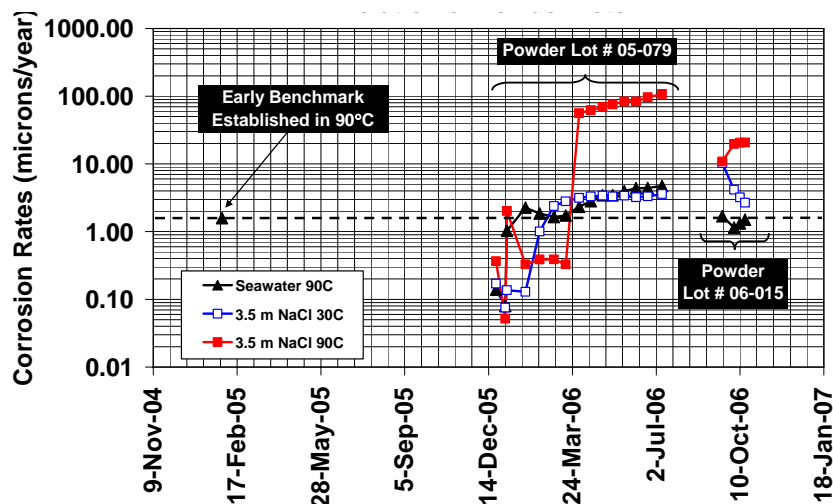

Figure 5. Apparent corrosion rates determined with linear polarization during long-term open circuit corrosion testing of as-sprayed SAM2X5 coatings prepared with lots of powder produced with Lot #05-079 and Lot #06-015 powders. A roughness factor of approximately 3.36 was used to convert current density to corrosion rate, to account for the rough as-sprayed surface.
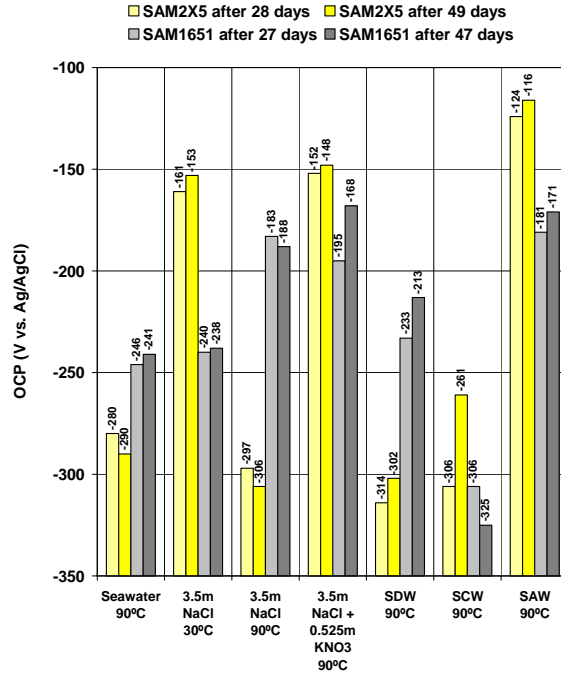
Figure 6. Comparison of OCP values for SAM2X5 and SAM1651 thermal spray coatings.
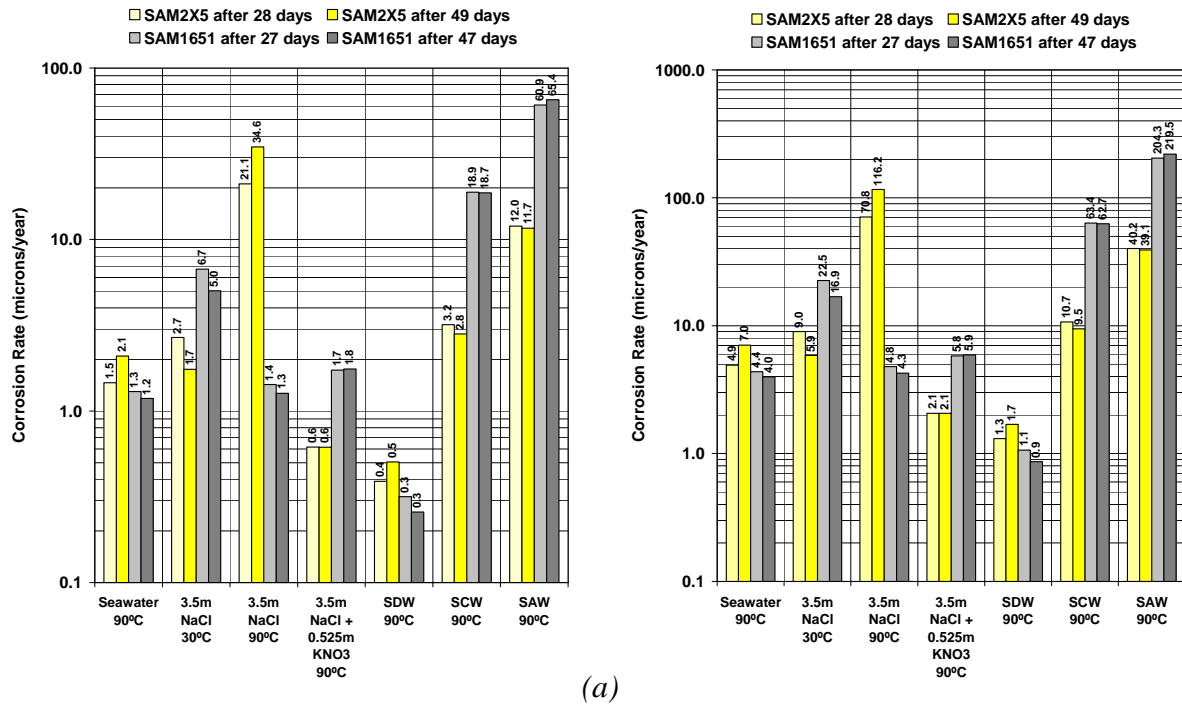

Figure 7. Corrosion rate values for as-sprayed SAM2X5 and SAM1651 coatings determined with linear polarization: (a) estimated roughness factor of approximately 3.36 assumed to account for the as-sprayed surface; and (b) no roughness factor assumed.

Conclusions

An iron-based amorphous metal, SAM2X5 ($Fe_{49.7}Cr_{17.7}Mn_{1.9}Mo_{7.4}W_{1.6}B_{15.2}C_{3.8}Si_{2.4}$), with very good corrosion resistance was developed. This material was produced as a melt-spun ribbon, as well as gas atomized powder and a thermal-spray coating. Chromium (Cr), molybdenum (Mo) and tungsten (W) provide corrosion resistance, and boron (B) enables glass formation. The high boron content of this particular amorphous metal make it an effective neutron absorber, and suitable for criticality control applications. Earlier studies have shown that ingots and melt-spun ribbons of these materials have good passive film stability. Thermal spray coatings of these materials have now been produced, and have undergone a variety of corrosion testing, including both atmospheric salt fog and long-term immersion testing.

After eight (8) full cycles in the standard GM salt-fog test, HVOF coatings of SAM2X5 on Type 316L stainless steel and nickel-based Alloy C-22 substrates demonstrated good resistance to corrosive attack in such environments. In contrast, reference samples of 1018 carbon steel were aggressively attacked, and were covered with a heavy layer of rust and corrosion product.

Linear polarization was used to determine the approximate corrosion rates of several amorphous-metal thermal spray coatings in a variety of potentially relevant environments. Coatings produced with completely amorphous SAM2X5 powder (Lot # 06-015) had relatively low corrosion rates in seawater at 90°C (~1.5 μm/yr). In contrast, coatings produced with partially devitrified SAM2X5 powder (Lot # 05-079) had relatively high corrosion rates (~4.7 μm/yr). Similarly, SAM2X5 coating samples produced with Lot # 06-015 powder exhibited relatively low corrosion rates in 3.5-molal NaCl solution at 90°C (~21.1 μm/yr), in comparison to those samples with Lot # 05-079 powder (~107.2 μm/yr). Measurements of linear-polarization corrosion rate in 3.5-molal NaCl solution at 30°C were very similar for SAM2X5 coating samples produced with Lots # 06-015 and # 05-079 (~2.7 and 3.6 μm/yr, respectively). Corrosion rates were determined in a broad range of environments. Based upon the corrosion rates of SAM2X5 coatings, solutions were ranked from least- to most-aggressive: SDW at 90°C; 3.5-molal NaCl with 0.525-molal KNO_3 solution at 90°C; seawater at 90°C; 3.5-molal NaCl solution at 30°C; SCW at 90°C; SAW at 90°C; and 3.5-molal NaCl solution at 90°C. The ranking for SAM1651 coatings was slightly different. SAM1651 performed better than SAM2X5 in hot 3.5-molal NaCl solution.

Acknowledgments

References

 [1]   M. Telford, The Case for Bulk Metallic Glass. *Materials Today*, Vol. 3, 2004, pp. 36-43

 [2]   N. R. Sorensen and R. B. Diegle, Corrosion of Amorphous Metals, *Corrosion, Metals Handbook*, 9th Ed., Vol. 13, edited by J. R. Davis and J. D. Destefani, ASME, 1987, pp. 864-870

 [3]   D. E. Polk and B. C. Giessen, Overview of Principles and Applications, Chapter 1, *Metallic Glasses*, edited by J. J. Gilman and H. J. Leamy, ASME, 1978, pp. 2-35

 [4]   K. Kishitake, H. Era, and F. Otsubo, Characterization of Plasma Sprayed Fe-10Cr-10Mo-(C,B) Amorphous Coatings, *J. Thermal Spray Tech.*, Vol. 5 (No. 2), 1996, pp. 145-153

 [5]   S. Pang, T. Zhang, K. Asami, and A. Inoue, Effects of Chromium on the Glass Formation and Corrosion Behavior of Bulk Glassy Fe-Cr-Mo-C-B Alloys, *Materials Transactions*, Vol. 43 (No. 8), 2002, pp. 2137-2142

 [6]   S. J. Pang, T. Zhang, K. Asami, and A. Inoue, Synthesis of Fe-Cr-Mo-C-B-P Bulk Metallic Glasses with High Corrosion Resistance, *Acta Materialia*, Vol. 50, 2002, pp. 489-497

 [7]   F. Guo, S. J. Poon, and G. J. Shiflet, Metallic Glass Ingots Based on Yttrium, *Metallic Applied Physics Letters*, Vol. 83 (No. 13), 2003, pp. 2575-2577

 [8]   Z. P. Lu, C. T. Liu, and W. D. Porter, Role of Yttrium in Glass Formation of Fe-Based Bulk Metallic Glasses, *Metallic Applied Physics Letters*, Vol. 83 (No. 13), 2003, pp. 2581-2583

 [9]   V. Ponnambalam, S. J. Poon, and G. Shiflet, *JMR*, Vol. 19 (No. 5), 2004, pp. 1320

 [10] D. Chidambaram, C. R. Clayton, and M. R. Dorfman, Evaluation of the Electrochemical Behavior of HVOF-Sprayed Alloy Coatings, *Surface and Coatings Technology*, Vol. 176, 2004, pp. 307-317

 [11] D. J. Branagan, Method of Modifying Iron-Based Glasses to Increase Crystallization Temperature Without Changing Melting Temperature, U.S. Pat. Appl. No. 20040250929, Filed Dec. 16, 2004

 [12] D. J. Branagan, Properties of Amorphous/Partially Crystalline Coatings. U.S. Pat. Appl. No. 20040253381, Filed Dec. 16, 2004

 [13] J. Farmer, J. Haslam, S. Day, T. Lian, C. Saw, P. Hailey, J-S. Choi, N. Yang, C. Blue, W. Peter, J. Payer and D. Branagan, Corrosion Resistances of Iron-Based Amorphous Metals with Yttrium and Tungsten Additions in Hot Calcium Chloride Brine and Natural Seawater, $Fe_{48}Mo_{14}Cr_{15}Y_2C_{15}B_6$ and W-containing Variants, *Critical Factors in Localized*

Corrosion 5, A Symposiun in Honor of Hugh Issacs, 210th ECS Meeting, edited by N. Missert, ECS Transactions, Vol. 3, ECS, 2006

[14] J. Farmer, J. Haslam, S. Day, T. Lian, C. Saw, P. Hailey, J-S. Choi, R. Rebak, N. Yang, R. Bayles, L. Aprigliano, J. Payer, J. Perepezko, K. Hildal, E. Lavernia, L. Ajdelsztajn, D. J. Branagan, and M. B. Beardsely, A High-Performance Corrosion-Resistant Iron-Based Amorphous Metal – The Effects of Composition, Structure and Environment on Corrosion Resistance, *Scientific Basis for Nuclear Waste Management XXX*, Symposium NN, MRS Symposium Series, Vol. 985, 2006

[15] T. Lian, D. Day, P. Hailey, J-S. Choi, and J. Farmer, Comparative Study on the Corrosion Resistance of Fe-Based Amorphous Metal, Borated Stainless Steel and Ni-Cr-Mo-Gd Alloy, *Scientific Basis for Nuclear Waste Management XXX*, Symposium NN, MRS Series, Vol. 985, 2006

[16] J-S. Choi, C. Lee, J. Farmer, D. Day, M. Wall, C. Saw, M. Boussoufi, B. Liu, H. Egbert, D. Branagan, and A. D'Amato, Application of Neutron-Absorbing Structural Amorphous Metal Coatings for Spent Nuclear Fuel Container to Enhance Criticality Safety Controls, *Scientific Basis for Nuclear Waste Management XXX*, Symposium NN, MRS Symposium Series, Vol. 985, 2006

[17] C. K. Saw, *X-ray Scattering Techniques for Characterization Tools in the Life Sciences, Nanotechnologies for the Life Science*, edited by Challa Kumar, Wiley-VCH Verlag GmbH and Company, KGaA, Weinheim, 2006

[18] C. K. Saw and R. B. Schwarz, Chemical Short-Range Order in Dense Random-Packed Models, *J. Less-Common Metals*, Vol. 140, 1988, pp. 385-393

[19] R. S. Treseder, R. Baboian, and C. G. Munger, Polarization Resistance Method for Determining Corrosion Rates, *Corrosion Engineer's Reference Book*, 2nd Ed., NACE, 1991, pp. 65-66

[20] J. E. Harrar, J. F. Carley, W. F. Isherwood, and E. Raber, *Report of the Committee to Review the Use of J-13 Well Water in Nevada Nuclear Waste Storage Investigations*, UCID-21867, LLNL, Livermore, CA, 1990

[21] G. E. Gdowski, *Formulation and Make-up of Simulated Dilute Water (SDW), Low Ionic Content Aqueous Solution*, YMP TIP-CM-06, Rev. CN TIP-CM-06-0-2, LLNL, Livermore, CA, 1997

[22] G. E. Gdowski, *Formulation and Make-up of Simulated Concentrated Water (SCW), High Ionic Content Aqueous Solution*, YMP TIP-CM-07, Rev. CN TIP-CM-07-0-2, LLNL, Livermore, CA, 1997

[23] G. E. Gdowski, *Formulation and Make-up of Simulated Acidic Concentrated Water (SAW), High Ionic Content Aqueous Solution*, YMP TIP-CM-08, Rev. CN TIP-CM-08-0-2, LLNL, Livermore, CA, 1997